Noise removal at the rod synapse of mammalian retina

Noise removal at the rod synapse of mammalian retina

M.C.W. VAN ROSSUM AND R.G. SMITH

Department of Neuroscience, University of Pennsylvania, Philadelphia

Abstract

Mammalian rods respond to single photons with a hyperpolarization of about 1 mV which is accompanied by continuous noise. Since the mammalian rod bipolar cell collects signals from 20–100 rods, the noise from the converging rods would overwhelm the single-photon signal from one rod at scotopic intensities (starlight) if the bipolar cell summed signals linearly (Baylor et al., 1984). However, it is known that at scotopic intensities the retina preserves single-photon responses (Barlow et al., 1971; Mastronarde, 1983). To explore noise summation in the rod bipolar pathway, we simulated an array of rods synaptically connected to a rod bipolar cell using a compartmental model. The performance of the circuit was evaluated with a discriminator measuring errors in photon detection as false positives and false negatives, which were compared to physiologically and psychophysically measured error rates. When only one rod was connected to the rod bipolar, a Poisson rate of 80 vesicles/s was necessary for reliable transmission of the single-photon signal. When 25 rods converged through a linear synapse the noise caused an unacceptably high false positive rate, even when either dark continuous noise or synaptic noise where completely removed. We propose that a threshold nonlinearity is provided by the mGluR6 receptor in the rod bipolar dendrite (Shiells & Falk, 1994) to yield a synapse with a noise removing mechanism. With the threshold nonlinearity the synapse removed most of the noise. These results suggest that a threshold provided by the mGluR6 receptor in the rod bipolar cell is necessary for proper functioning of the retina at scotopic intensities and that the metabotropic domains in the rod bipolar are distinct. Such a nonlinear threshold could also reduce synaptic noise for cortical circuits in which sparse signals converge.

Keywords: Rod bipolar, mGluR6 receptor, Threshold nonlinearity, Photon detection

Introduction

Convergence of many synaptic inputs onto a neuron's dendritic tree is common in the nervous system, but it introduces a problem. Even minor amounts of noise, when compounded by convergence, can increase the neuron's noise level to a point where the signal is overwhelmed. The problem is particularly severe for sparse signals, i.e. where signals from separate synaptic inputs do not overlap in time. However, in this case a nonlinear processing step can remove noise to maintain signal quality. We present here an account of how such nonlinear processing can improve rod signal quality in the retina.

Mammalian rods respond to a single photon with a hyperpolarization of about 1 mV (Baylor et al., 1984; Tamura et al., 1989; Schneeweis & Schnapf, 1995). The single-photon signal is known to be transmitted as a separate event by the retina to the brain because it has been detected in ganglion cell spike trains as a burst of 2–3 spikes (Barlow et al., 1971; Mastronarde, 1983). The single-photon signal has also been demonstrated in the ERG (Robson & Frishman, 1995) and psychophysically (Sakitt, 1972; but see

Makous, 1990). This implies that retinal circuitry in transmitting the single-photon signal preserves its quantal identity.

A sequence of neurons called the "rod bipolar pathway" carries rod signals at night (Famiglietti & Kolb, 1975; Nelson, 1982), and appears to be specialized to transmit the single-photon signal (Sieving et al., 1986; Smith et al., 1986; Robson & Frishman, 1995; Smith & Vardi, 1995). At low scotopic intensities (starlight) only one rod in 1000 absorbs a photon per second, so to concentrate the signal the circuit sums rod signals through anatomical convergence. The rod bipolar cell receives glutamatergic synaptic input from 20–100 rods, depending on species and retinal eccentricity (Dacheux & Raviola, 1986; Young & Vaney, 1991; Wässle et al., 1991; Grünert et al., 1994). Although the physiological and anatomical details of the rod bipolar pathway differ across species, the basic pattern is the same: in starlight both rod and rod bipolar process the signal from at most one photon.

Recordings from single mammalian rods show that the single-photon response is accompanied by noise (Baylor et al., 1984; Schneeweis & Schnapf, 1995), which is thought to originate in the biochemical transduction cascade (Baylor et al., 1980) shared by vertebrates. The spectrum of the noise measured in fish, toad, and monkey is similar to that of the photon signal, therefore the noise cannot be removed by a temporal filter (Ashmore & Falk, 1982; Baylor et al., 1980, 1984). The standard deviation of the noise in monkey is 19% ± 5% of the peak of the single-photon response,

yielding a signal-to-noise ratio of about 5 (Baylor et al., 1984; Schneeweis & Schnapf, 1995).

On first thought, a signal-to-noise ratio of 5 in a rod might seem quite reasonable. However, Baylor et al. (1984) pointed out that if signals from many rods converge on the bipolar cell and are linearly summed, noise from surrounding rods would overwhelm the signal from a single photon transduced in one rod. The reason is that the standard deviation of summed noise is proportional to the square root of the number of independent noise sources. Although electrical coupling of photoreceptors can increase the signal-to-noise ratio in some cases, for the single photon signal it does not (Tessier-Lavigne & Attwell, 1988). Indeed, mammalian rods are not coupled (Raviola & Gilula, 1973; Schneeweis & Schnapf, 1995). Hence noise from the 20 rods converging onto a single rod bipolar cell in cat retina would mask an individual single-photon signal, and the noise from the 1500 rods converging onto a central beta (X) ganglion cell (Sterling et al., 1988) would completely swamp it! Baylor et al. (1984) therefore proposed a nonlinear threshold somewhere at the rod → rod bipolar synapse.

Synaptic noise further worsens the noise problem. In the dark, a rod is depolarized and vesicles of glutamate are thought to be released continuously (Trifonov, 1968; Cervetto & Piccolino, 1974; Kaneko, 1979; Detwiler et al., 1984). Since release is thought to be random (Stevens, 1993), it is an additional source of noise that varies with the vesicle release rate (Rao et al., 1994). Finally, the postsynaptic ion channels fluctuate randomly, so they are a source of noise that varies with the degree of activation (de la Villa et al., 1995). Thus, there are at least three sources of noise that could mask the quantal identity of a single-photon signal in the rod bipolar.

A likely candidate for the thresholding mechanism is the mGluR6 receptor and associated biochemical second-messenger cascade located at the dendritic tip of the rod bipolar cell at its glutamatergic synapse with the rod (Shiells & Falk, 1990; Yamashita & Wässle, 1991; Vardi et al., 1993; de la Villa et al., 1995). Recently, Shiells and Falk (1994) measured the response of an mGluR6-driven bipolar cell in dogfish retina to variations in the concentration of glutamate and discovered a nonlinearity in its response: at high concentrations of glutamate (i.e. low light levels) all the postsynaptic ion channels closed. Below a threshold glutamate concentration the synaptic conductance strongly increased.

One might choose to study the rod synapse in mammalian retina physiologically by recording from a rod bipolar cell in a dark-adapted slice preparation. Whole-cell patch recording might reveal single-photon responses and provide evidence for a nonlinearity, but this would be an extremely difficult experiment. A simpler experiment would be to patch an isolated rod bipolar cell without rod synapses intact and record responses to glutamate puffs (Yamashita & Wässle, 1991; Shiells & Falk, 1994; de la Villa et al., 1995). But this could not provide evidence about the single-photon response nor the influence of noise from rod and synapse.

Therefore, to measure the performance of the rod → rod bipolar circuit in the presence of different types of noise, we chose a computer simulation. We included realistic models of the rod signal, continuous dark noise, and a rod synapse with random vesicle noise, second-messenger cascade and nonlinearity. This approach required assumptions for some physiological parameters, but on the other hand allowed us to study the effect of parameter variations on the performance of the system. The objectives were (1) to estimate the vesicle release rate because that was an important determinant of noise in the model, (2) to explore the contribution of the different noise sources on single-photon detection, and (3) to

discover whether the mGluR6 threshold nonlinearity would allow single-photon detection in the rod bipolar pathway.

Methods

As a preliminary study, we derived an analytical model and compared the performance for rods converging onto the rod bipolar through a linear and through a nonlinear thresholding synapse (Appendix). The results show that with the linear synapse, the single-photon signal is lost in the numerous errors and that a threshold is very effective in reducing detection errors when multiple rods converge. For this model, we assumed that the input noise at every synapse was Gaussian (its width set so the error rate met our error criteria, see below), and that the threshold was ideal. These few assumptions are not easily justifiable and the results might not hold if the noise were modeled more realistically and the threshold were provided by a realistic second-messenger cascade. The combination of nonlinearities and temporal filters makes analytical treatment cumbersome. Therefore, we studied the system with a compartmental model.

We simulated the rod → rod bipolar circuit using the simulation language "NeuronC" (Smith, 1992). The architecture of the circuit and the physiological parameters were defined in a script file. The model consisted of an array of up to 25 rods, one bipolar cell, and one horizontal cell axon terminal; see Fig. 1. The horizontal cell with a synapse to each rod was included to provide a conductance to appropriately set the rod resting voltage (analogous to feedback from horizontal cells *in vivo*; see "Setting the threshold" in the Discussion). For simplicity, the horizontal cell voltage was manually set to a constant value (Lankheet et al., 1996).

A stimulus consisting of a series of dim flashes was presented to the array of rods. In real photoreceptors photon absorption occurs randomly (e.g. Schneeweis & Schnapf, 1995), but for simplicity each simulated flash caused exactly one photon absorption. The absorption caused an outward current of about 1 pA, leading to a hyperpolarization with a peak amplitude of about 1 mV. Transduction in the rod was modeled with a 7th-order equation based on an enzyme cascade as postulated by Pugh and Altman (1988). The decay phase consisted of a 4th-order equation, modeling the calcium feedback (for details see Smith, 1992). The resulting single-photon response (Fig. 2) was similar to the one measured by Baylor et al. (1984). The continuous dark noise of the rod was modeled by inserting noise in the transduction cascade. At the rod output, the noise had a Gaussian distribution with a power spectral density comparable to the single-photon response (Fig. 2).

Synapse

We modeled the synapse from rod-to-rod bipolar as a sequence of functions based on the work of Belgum and Copenhagen (1988), where the presynaptic voltage directly modulates a postsynaptic conductance. To generate realistic postsynaptic responses with appropriate noise properties, we added to this model (1) discrete vesicle release, (2) temporal filters to insert time delays and shape the postsynaptic response, and (3) a second-messenger cascade, see Figs. 3 and 4 (Smith, 1992). Each filter in the synapse consisted of a number of low-pass filters with equal time constants in series. The impulse response of such a compound filter is

$$F(t) = \frac{t^{n-1}e^{-t/\tau}}{(n-1)!}, \qquad (1)$$
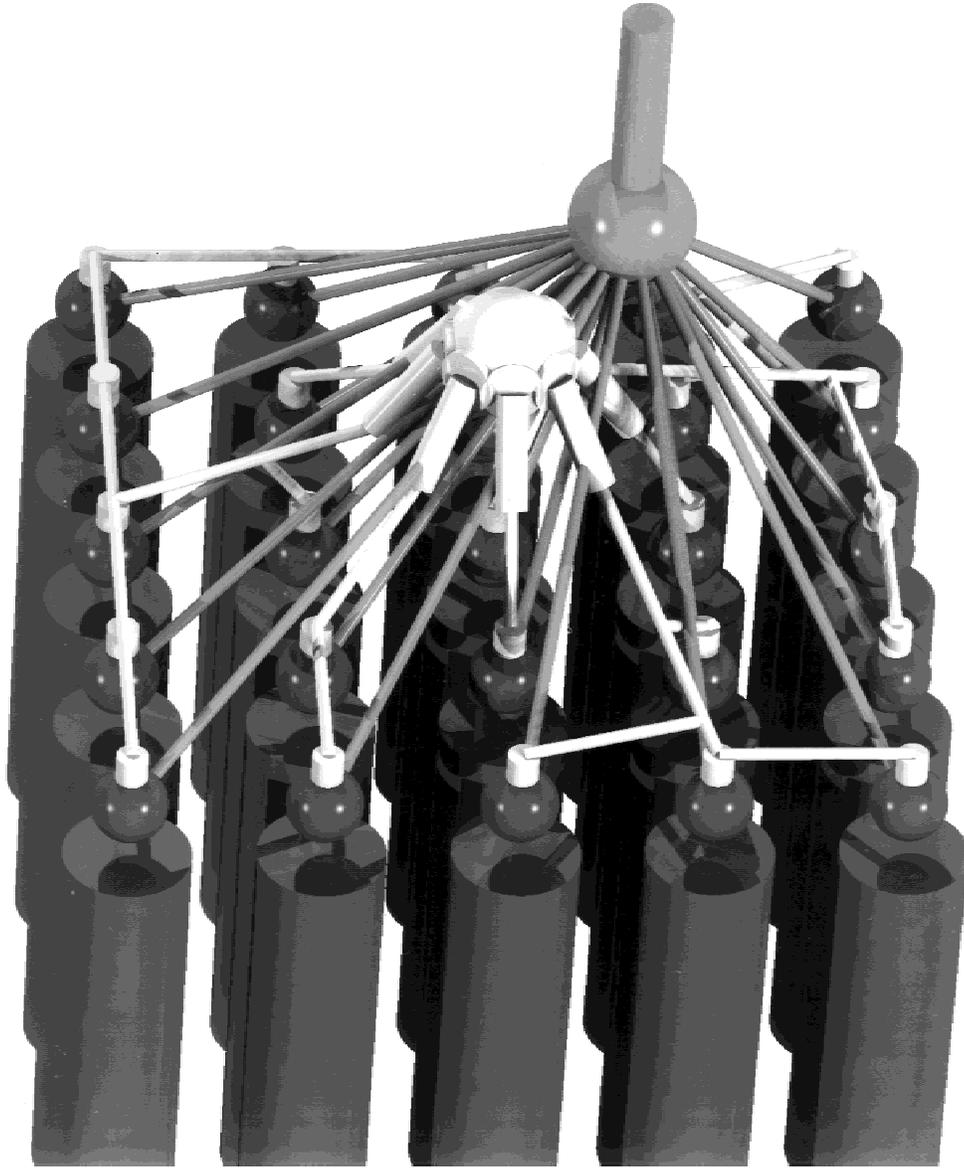
Fig. 1. Model of the rod bipolar circuit, containing 25 rods, one horizontal cell (light gray center cell) and on top a rod bipolar cell.

where n is the number of filters in series, and τ is the time constant.

The temporally filtered rod voltage modulated the average rate of release, $\rho(t)$, with an exponential function (Belgum & Copenhagen, 1988)

$$\rho(t) = \rho_0 e^{[V_{\text{rod}}(t) - V_{\text{dark}}]/V_e}, \qquad (2)$$

where V_{rod} is the rod voltage and V_{dark} is the average dark voltage of the rod. The prefactor ρ_0 sets the vesicle release rate in the dark. V_e gives the exponent of transmitter release and determines the ratio of the release rates in the dark and with one photon absorbed. Although the rod $\rightarrow$ rod bipolar synapse might transmit a two-photon signal (see Discussion), we assumed that a single-photon signal almost completely stopped vesicle release. This enhanced performance by more fully exploiting the dynamic range of the synapse, reducing the relative contribution of noise. Since the precise vesicle

release behavior is not known, we chose to err here towards better performance to strengthen the conclusions (see Results).

Given the rate, vesicle release was modeled as a modulated Poisson process (Katz & Miledi, 1965; Barrett & Stevens, 1972*a*,*b*; Stevens, 1993). Poisson release corresponds to exponentially distributed release intervals. It might be realistic, however, to assume that vesicle release events have some refractory time (time during which release is blocked). At low release rates when the rod absorbs a photon and hyperpolarizes, the time between releases will be much larger than a refractory time, and a Poisson approximation is appropriate. In the dark, however, when the rod tonically releases glutamate at a high rate, the refractory time might become comparable to the intervesicle time. In that case, a refractory time would regularize the release and lower the number of errors compared to Poisson release at the same rate (Laughlin et al., 1996). From a biological point of view, a fixed refractory time does not seem realistic, so vesicle release was modeled with a gamma dis-
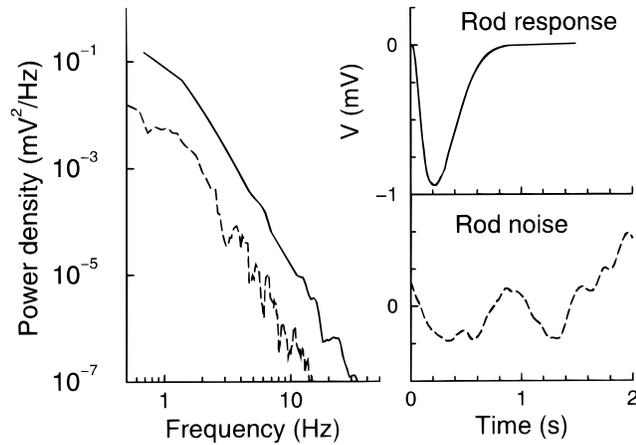
Fig. 2. Left: The power spectral densities of the single-photon response (solid line) and the noise (dashed line). Right: simulated rod response to a single photon in the absence of continuous dark noise (upper graph) and a simulated trace of the continuous dark noise (lower graph).

tribution of interval times, i.e. the interval times are distributed according to (Abramowitz & Stegun, 1965)

$$p(t_i) = \rho(\rho t_i)^{k-1} e^{-\rho t_i} / (k-1)! \tag{3}$$

The gamma distribution has both a rate parameter ρ and an order k. If k is one, the interval distribution is exponential and generates the Poisson event distribution. For large gamma order the release is more regular. The coefficient of variation (standard deviation/mean) of the number of events per unit time is a factor $\sqrt{k}$ smaller than for Poisson release, thus regularizing the release.

Second-messenger cascade

The rod bipolar of mammals utilizes the mGluR6 receptor at the glutamatergic synapse with the rod (Shiells & Falk, 1990; Wässle et al., 1991; Vardi et al., 1993). The mGluR6 receptor modulates a second-messenger system similar to the transduction cascade in photoreceptors. Glutamate binds to the postsynaptic receptors and
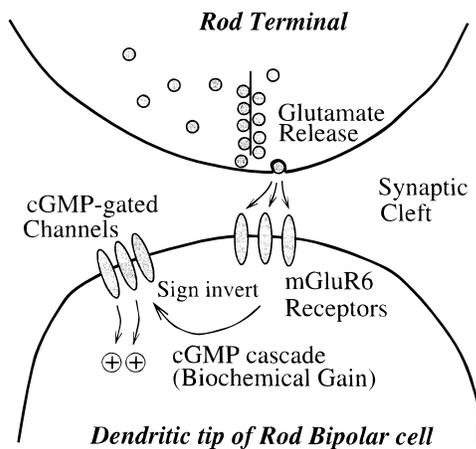
Fig. 3. Schematic of the rod → rod bipolar synapse.

leads to a reduction in cyclic GMP (cGMP) which closes the depolarizing channels in the rod bipolar dendritic membrane (Nawy & Jahr, 1990, 1991; Shiells & Falk, 1994; de la Villa et al., 1995). We modeled this following Shiells and Falk (1994). The temporal filters are omitted here for clarity, but in the simulation they were present as specified in Fig. 4.

$$[Glu]_{\text{bound}} = \frac{[Glu]_{\text{cleft}}}{[Glu]_{\text{cleft}} + k_1}, \tag{4}$$

$$[cGMP] = 1 - c_{\text{gain}} \cdot [Glu]_{\text{bound}}, \qquad \text{but } [cGMP] \geq 0 \tag{5}$$

$$g = g_{\text{syn}} \frac{[cGMP]}{[cGMP] + k_2}, \tag{6}$$

where $[Glu]_{\text{cleft}}$ is the glutamate concentration in the synaptic cleft resulting from the random release. $[Glu]_{\text{bound}}$ is the amount of receptor bound glutamate, k_1 sets Michaelis-Menten saturation of the glutamate binding. c_{gain} is the biochemical gain of the cascade. k_2 sets the saturation for cGMP, its value taken from Shiells and Falk (1994). Finally, g and g_{syn}, represent the synaptic conductance of the bipolar cell and the maximal synaptic conductance. The threshold works the following way: As long as $c_{\text{gain}} \cdot [Glu]_{\text{bound}} > 1$, the cGMP concentration is zero as it cannot become negative. If $c_{\text{gain}} \cdot [Glu]_{\text{bound}} < 1$, the cGMP concentration follows inversely the variations of the glutamate concentration. It thus shows a thresholding behavior at high glutamate concentrations. Note that by eqn. (4) the maximal value of $[Glu]_{\text{bound}}$ is normalized to one and thus c_{gain} has to be larger than one to obtain the thresholding behavior. Due to the threshold, fluctuations in the rod voltage in the dark do not cause a response in the bipolar cell. This is the mechanism responsible for noise removal in the simulation.

In some simulation runs we included channel noise. Assuming a synaptic conductance of 100–200 pS and a single-channel conductance of 13 pS (de la Villa et al., 1995), each dendritic tip would contain 8–16 channels. The noise of the channels was modeled by a binomial distribution (N = number of channels, p = normalized conductance) which was filtered with a first-order low-pass filter with a cutoff frequency of 47 Hz (de la Villa et al., 1995).

To examine the effect of the nonlinearity in the simulations we set the synapse parameters for two different types of transfer function (the function relating presynaptic voltage to postsynaptic conductance). In the first, we set a central linear zone, and in the second, we set a strong thresholding nonlinearity (Fig. 5). Some nonlinear behavior is also caused by the vesicle release function and the glutamate binding constant k_1 (at high glutamate concentrations) and the cyclic G binding constant k_2 (at the shoulder of the solid curve in Fig. 5), but the thresholding effect is set by the nonlinearity of the postsynaptic second-messenger cascade.

Analysis of signal in rod bipolar

The output of the compartmental simulation was the voltage recorded from the rod bipolar soma. After an adjustable latency the voltage was integrated with a matched filter over 100 ms, representing the integration time of the bipolar. The integration time was determined from two measurements: the AII amacrine cell rises to half-maximum in 90 ms (Nelson, 1982), and the time to
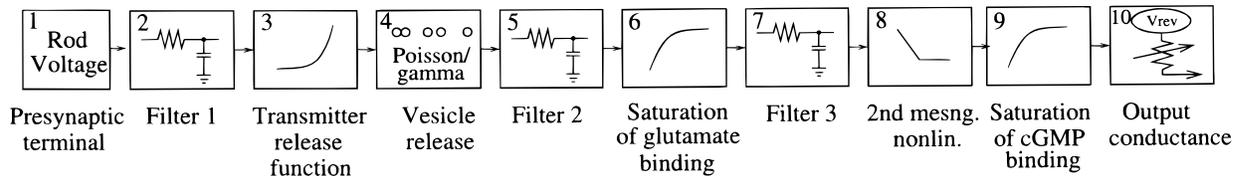
Fig. 4. Simulation of the synapse. Box 2: Voltage of the rod is temporally filtered. 3: Synaptic gain is controlled by changing the steepness and voltage offset of the exponential release function. 4: Vesicles are randomly released according to the model for release. 5: The pulse of transmitter from a vesicle is shaped in the second filter which represents the smearing of the concentration due to diffusion and the dynamics of the binding of glutamate to the receptor. 6: The transmitter binds postsynaptically, saturating according the Michaelis-Menten law. 7: Delay in the action of the bound transmitter is represented with the third filter. 8: The cGMP concentration is a nonlinear function of the amount of receptor bound glutamate. 9: Saturation in binding of cGMP to ion channels. 10: Modulated postsynaptic conductance. See text and Table 1 for parameter values.

peak measured in cat rod bipolar ERG measurements is about 100 ms (Robson & Frishman, 1995). A matched filter has an impulse response which is a time-reversed version of the signal to be detected. This filter maximizes the signal-to-noise ratio of the output if the signal to be detected is known and embedded in white noise (Davenport & Root, 1958; Baylor et al., 1980). The shape of the filter was determined by averaging the bipolar voltage response to a photon. Although the matched filter improves the detection compared to a rectangular, unweighted integration window if the integration time is long (>400 ms), for the 100-ms integration the effect was small (always less than 1%), which was expected because the signal was slow compared to the 100-ms time window of the filter.

The filtered rod bipolar voltage was compared to a preset discrimination voltage. If the bipolar voltage was above (below) discrimination voltage, it was decided that a (no) photon was detected by the rod bipolar. After a photon was detected, the detection was suspended for 100 ms in order not to count accidentally the tail of the event as a second photon. To correctly calculate the photon rates, this "dead time" was subtracted from the total time.
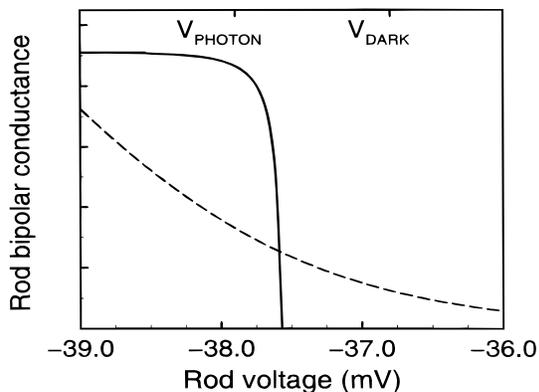
Fig. 5. Static transfer functions of the rod synapse. When the rod absorbs a photon it hyperpolarizes, glutamate release drops, and the conductance of the bipolar cell increases. Depending on synaptic parameters (synaptic gain, voltage offset, and second-messenger gain c_{gain}) the synapse shows a strong thresholding behavior (solid line, $c_{gain} = 3$) or an almost linear behavior (dashed line, $c_{gain} = 1$).

Measuring error rates

Because of the signal's binary character, we quantified the performance of the system in false positive and false negative rates instead of a signal-to-noise ratio. A false positive is the detection of a photon when there is none (measured in false positives per second); a false negative is missing a photon (measured in fraction of photons missed). The false positive and false negative rates are mutually exclusive: by increasing the discrimination voltage for the signal in the rod bipolar it is possible to arbitrarily reduce the false positive rate at the expense of a higher false negative rate (see Fig. 9).

Since obvious goals of the retina are to maximize efficiency and reduce errors, we set limits for the false negative and false positive rates with the following reasoning. The efficiency factor for the single-photon signal describing the fraction of rhodopsin isomerizations detected in the discriminator equals one minus the false negative rate. To maximize efficiency, therefore, the false negative rate should be as low as possible. To minimize errors, however, a low false positive rate is necessary. For simplicity, we fixed the false negative rate and measured the false positive rate (Figs. 9 and 10). These rates were controlled in the simulation by varying the discrimination voltage in the rod bipolar cell. Permissive values (i.e. allowing errors) were chosen for the limits but we imagine that the retina might well have more stringent limits, especially since noise from higher order neurons was not included. The efficiency of a ganglion cell has been estimated at 70% which corresponds to a false negative rate of 30% (Mastronarde, 1983). To set a permissive value we posed the condition: (1) *The false negative rate caused by intrinsic noise should be less than 50% missed photons.*

The limit on the false positive rate is provided by the dark event rate, which originates from spontaneous, thermal rhodopsin isomerizations causing rod responses indistinguishable from photon responses. Thus dark events pose a fundamental visual performance limitation. From direct rod recordings the number of dark light events is (0.0063 ± 0.0018) Rh*/rod/s in monkey (Baylor et al., 1984). On the other hand, ganglion cell recordings in the cat yielded 2–6 events/ganglion cell/s (Mastronarde, 1983), and 5.5 photon events per ganglion cell/s (Barlow et al., 1971) which is consistent with a dark event rate of about 0.005 events/rod/s (Sterling et al., 1988). Psychophysical experiments yielded 0.01 events/rod/s (Lamb, 1990; Frishman et al., 1996). Thus, the dark event rate in ganglion cells seems to stem from the dark event rate in the rods, and the retinal circuitry itself apparently introduces few errors. As a permissive criterion, we posed the condition that the

errors are less than the spontaneous dark events: (2) *The false positive rate caused by dark continuous noise and vesicle noise should be less than 0.01 events/rod/s.*

Results

Simulation of single rod

In the first set of simulations just one rod was connected to the rod bipolar cell (Table 1). Parameters for the simulation were taken from the literature where known. When there was an uncertainty in a parameter value, we chose to err towards a value which improved performance. If under these more optimal conditions the error rates of the system with the linear synapse were too high, that would better demonstrate the necessity of the nonlinearity. Parameters chosen this way were (1) the vesicle release function, set so that a single photon stopped vesicle release; (2) the integration time of the bipolar cell and of the discriminator, set to be as long as compatible with physiological recordings; and (3) the latency in the discriminator, set to minimize the error rate.

The rod inner segment consisted of a sphere (8 μm diameter) synaptically connected to a dendrite (0.2 μm diameter) of the rod bipolar cell. The rod bipolar had a soma represented by a sphere (5 μm diameter) and an axon of 0.8 μm diameter (Fig. 1). The membrane resistance of the rod was set to give a single-photon response of about 1 mV. Conductances included (1) the synaptic conductance and (2) a nonspecific conductance represented by R_m with a reversal potential of -70 mV for both rod and rod bipolar. The synaptic conductance g_{syn} was set to 200 pS, but its precise value was not important as the error detection by the discriminator was independent of the amplitude of the bipolar voltage. Noise from the fluctuation of synaptic channels comprised high frequencies which were filtered out by the time window, and gave a negligible contribution to the error rate (see Discussion). Therefore channel noise was not included in the simulation beyond the initial runs.

The synaptic temporal filters were chosen as follows: the first filter was second-order with a short time constant to give a presynaptic delay, consistent with the delay in vesicle release (Barrett & Stevens, 1972*a*). The second filter (representing the diffusion and binding to the receptors) was second order to match the shape of the time course of diffused neurotransmitter; the time constant was consistent with mPSCs measured in OFF bipolar cells (Maple

et al., 1994). The last filter, representing the temporal integration of the second-messenger cascade, was third order, consistent with the number of integration stages measured in the rod bipolar cell (Robson & Frishman, 1995). Its function was to filter out the high-frequency components of the vesicle noise before they were passed through the threshold. The time constant of the filter was set to 50 ms, compatible with the time course of the bipolar response (Dacheux & Raviola, 1986). A shorter time constant increased the error rate. The response of the synapse to one vesicle shows the inverting of the signal and the long time constant of the response (Fig. 6).

At fixed time intervals the rod received a photon. The response of the rod was a small hyperpolarization superposed on the continuous dark noise. An inverting glutamatergic synapse transmitted the signal and noise to the bipolar cell (Fig. 7).

The bipolar cell signal was temporally integrated over 100 ms with a matched filter (see Methods). A fixed time delay was added to the stimulus representing the latency of the bipolar cell. For every set of simulation parameters, this delay was optimized for the lowest false positive rate; a delay of 150 ms was common. The filtered bipolar cell signal was compared to a preset discriminator threshold voltage. An excursion above the threshold was taken to be a photon. A comparison to the actual stimulus categorized the photon as a "real" or a "false" photon. While the false negative rate was kept fixed at 50%, the false positive rate of the circuit was determined for various values of the noise parameters. For low false positive rates, long simulations with few photons were necessary to obtain a sufficient number of false positive events (over 1 h of modeled time with about 1 photon per 3 s per rod).

For a single rod connected to the bipolar cell, there was no significant difference in performance between the linear and the thresholding synapse. The reason is that a nonlinear threshold in the synapse has an effect similar to the discriminator. With the signal provided by only one source, the classification of responses into "photon" or "no photon" is unchanged whether or not the signal passes through a prior nonlinear threshold.

For a standard deviation of the continuous rod dark noise equal to 19% of the peak response, a Poisson rate of at least 80 vesicles/s was necessary to keep false positives below 0.01/rod/s (Fig. 8). This minimal estimate served as a calibration for the simulations with multiple rods. The minimal rate depended strongly on the distribution of release times. For a gamma distribution of order 4, the minimal rate was about 40 vesicles/s (Fig. 8).

Table 1. *Parameters in the compartmental simulation*

Parameter	Value	Reference
Membrane resistance rod	6000 Ωcm^2	
Membrane capacity	1 μF/cm^2	
Synaptic filter 1, order	2	
Synaptic filter 1, time constant	0.2 ms	(Barrett & Stevens, 1972*a*)
Synaptic filter 2, order	2	
Synaptic filter 2, time constant	2 ms	(Maple et al., 1994)
Synaptic filter 3, order	3	(Robson & Frishman, 1995)
Synaptic filter 3, time constant	50 ms	
c_{gain} (linear)	1	
c_{gain} (threshold)	3	
Max. synaptic conductance g_{syn}	200 pS	(de la Villa et al., 1995)
Synaptic rev. potential	0 mV	(de la Villa et al., 1995)
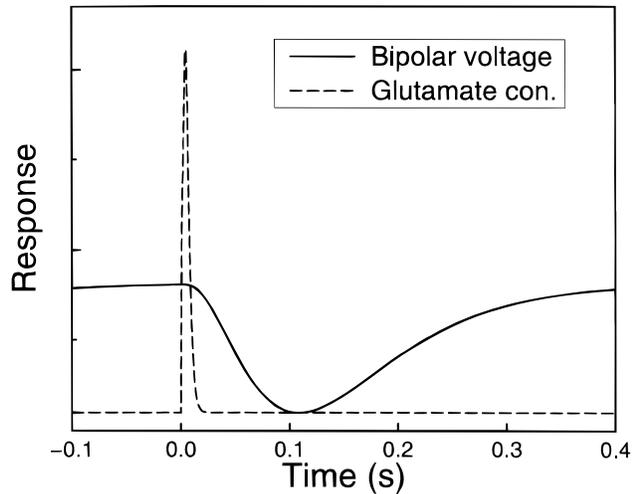
Fig. 6. The response to a single vesicle showing the effect of the temporal filtering in the synaptic model. Dashed line: the filtered glutamate concentration (output of second filter). Solid line: the voltage response in the bipolar cell.

Simulation of multiple converging rods

Next, the number of rods connected to the bipolar cell was increased (4, 9, 16, and 25 rods). The dark vesicle rate was set to 100 vesicles/s and the dark noise was set to 19%, other parameters were the same as for the single rod simulation. Without thresholding, the standard deviation of the voltage distribution in the bipolar was much larger than the standard deviation for a single rod. When the threshold was present, it transformed each rod bipolar voltage distribution into two narrow peaks and allowed the single-photon signals to remain detectable (Figs. 9 and 10).

For the linear synapse, the false positive rate increased strongly with the number of rods converging (Fig. 11). When the simulations included only vesicle release noise or continuous dark noise the false positive rate for the linear synapse was still larger than for the thresholding synapse. The continuous dark noise and vesicle release noise contributed both considerably to the false positive rate with a somewhat larger contribution of the vesicle release noise. For the thresholding synapse, the false positive rate was much lower and proportionate to the number of rods converging, except for 25 rods where the false positive rate was somewhat larger than the dark light.

For very large amounts of noise, the voltage distributions for dark rods and for one rod capturing a photon fully overlapped (Fig. 10). The false positive rate was at that point 1 minus the false negative rate, i.e. 50%. In our model only one event could be detected per integration time (100 ms); the false positive rate therefore saturated at 5 events/s.

Discussion

The results show that continuous dark noise in rods and vesicle fluctuation noise at the rod synapse leads to errors in photon detection (false positives and false negatives). We found that if rod signals were summed linearly by the rod bipolar, it could not reliably transmit the single-photon signal, as the false positive rate increased rapidly with the number of converging rods to an unacceptably high level. Our results show that a thresholding non-

linearity is effective for reducing the false positives to a rate consistent with physiological measurements (Barlow et al., 1971; Mastronarde, 1983).

Performance of circuit with single rod convergence

We found a minimal release rate of about 80 vesicles/s for the case of Poisson release both with the linear and the thresholding synapse. This was obtained by considering one rod synaptically connected to the rod bipolar. Since convergence further adds to the noise, this rate is also a minimum estimate for the circuit with multiple rods. It is comparable to the value of 40/s estimated by Rao et al. (1994) and 100/s in more recent work (Rao-Mirotznik & Sterling, 1998), where the problem of convergence was not fully considered. Comparable experimental values have been found by Ashmore and Copenhagen (1983), von Gersdorff et al. (1996), and Freed (1998). Higher rates of vesicle release would improve the performance of the system, but continuous rates much higher than 100/s are thought to be biologically implausible (Rao-Mirotznik & Sterling, 1998). The estimated rate depends on the integration time of the bipolar cell. A longer integration time allows a lower release rate at the expense of a longer latency for detecting a photon.

Performance of circuit with multiple rod convergence

Summing multiple-photon signals from a pool of rods leads to an increase in noise in the rod bipolar signal (Fig. 9). When the synapse is linear the noise prevents the circuit from successfully discriminating single photons (Figs. 10 and 11). The effect is also present with either the continuous dark noise or the vesicle release noise alone, indicating that it does not critically depend on our estimate of the dark vesicle rate or properties of the dark noise.

Although the nonlinear threshold does not improve the performance of the circuit with one rod, it does improve the performance when multiple rods converge. The threshold blocks noise from rods which do not carry a photon signal. This greatly reduces the noise pooled by the rod bipolar, which improves its performance to a false positive rate comparable to the known dark rate (0.01/rod/s). The threshold improves the performance so much that the circuit with both rod and vesicle noise has better performance than it would have with a linear synapse and either noise source alone (Fig. 11).

Essential features of the model

The results of the analytical model (Fig. 13) are similar to the simulation data (Fig. 11). This emphasizes that although the precise error rates may depend on the model, the conclusion that thresholding is a necessity follows from both models. Most of the physiological and anatomical parameters in the compartmental simulation are not critical. For the proper functioning of the circuit, however, it is essential that (1) the threshold removes the noise of the dark rods, because they are the majority and would otherwise contribute strongly to the noise. This is consistent with the working of the mGluR6 cascade which did not respond to fluctuations above a certain glutamate level; in the analytical model noise in the presence and absence of signal are removed. (2) The threshold voltage is accurately set to balance the noise removal against transmission of the photon signal (see below). In the model, this was done by setting the threshold voltage either by changing the horizontal cell feedback or changing the synapse parameter k_1. (3) The vesicle noise is filtered out. It contains high-frequency com-
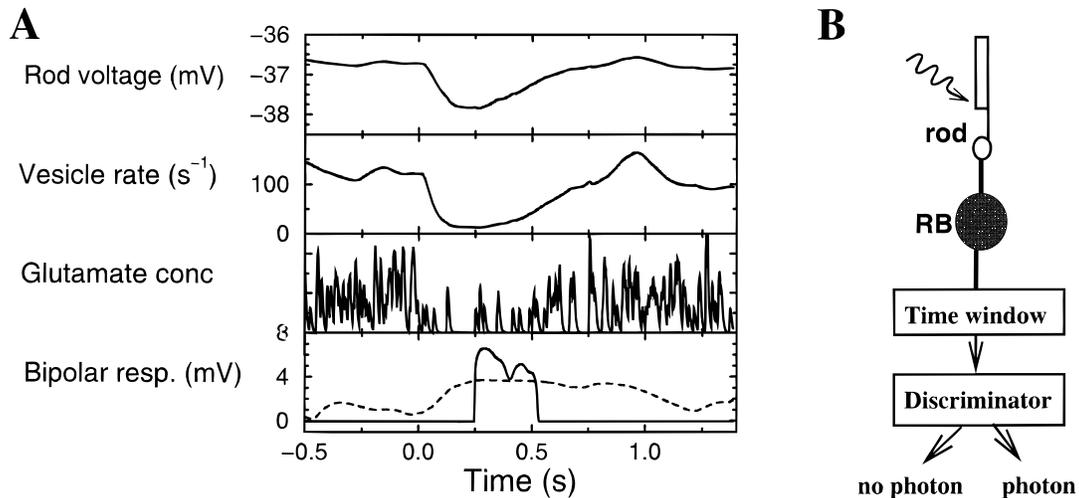
Fig. 7. (A) Trace of a simulation with one rod connected to the bipolar cell with linear and threshold synapse. At $t = 0$, a photon was absorbed by the rod. Note the continuous dark noise fluctuations in the rod voltage, and the vesicle noise in the glutamate concentration (about 100 vesicles/s, Poisson release). The rod bipolar response is shown for the linear (dashed line) and the thresholding synapse (solid line). (B) Analysis of the bipolar voltage: after a 100-ms filter, the signal is compared with a discrimination voltage. Comparison to the stimulus yields the error rate.

ponents that otherwise would be passed by the nonlinearity. In the simulation, the third filter performed this task; it was not relevant for the analytical model which did not contain dynamics. (4) The threshold is located after most of the noise sources, but before the summation of the rod inputs.

Location of nonlinearity

If the nonlinearity were located in the presynaptic terminal, e.g. a voltage-gated channel in the rod terminal, it could reduce the continuous rod noise but could not reduce vesicle fluctuation noise. If,
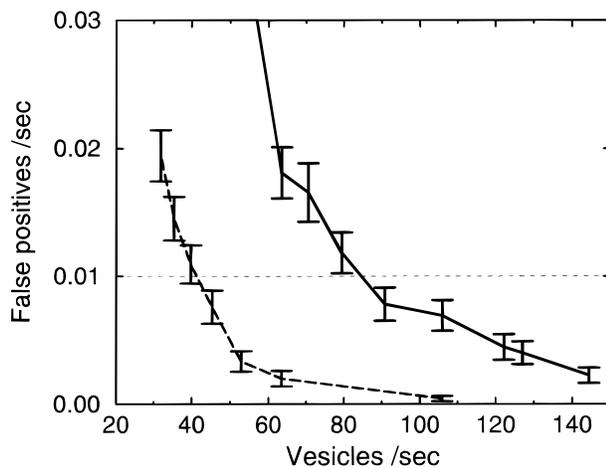

Fig. 8. The false positive rate for a single rod connected to the rod bipolar cell. Solid line: Poisson release, about 80 vesicles/s minimum are necessary to yield a low enough false positive rate (thin horizontal line). Dashed line: gamma distributed intervesicle time of order 4, having a standard deviation half that of Poisson release at the same rate. In that case 40 vesicles/s are sufficient. The dark noise was set to 19%. Data were collected from about 1 h of simulated time in which some 1000 photons were absorbed.

on the other hand, the nonlinearity were located in the rod bipolar soma or axon, it might reduce noise to some extent but could only process photon signals already embedded in the pooled noise from 20 other rods. To be most effective, the nonlinearities in the bipolar cell should be distinct and independent. Therefore the postulated threshold would be optimally located in the postsynaptic side of the synapse, which is consistent with the location of the mGluR6 cascade in the bipolar cell (Wässle et al., 1991; Vardi et al., 1993; de la Villa et al., 1995).

To be independent, the second-messenger cascades in the dendritic tips of a rod bipolar cell must be localized and therefore limited in scale. The noise from a small number of channels can be large, but it diminishes when all channels are open or all channels are closed (de la Villa et al., 1995). Furthermore, the noise comprises high frequencies which are filtered out by the discriminator. In simulation runs that included channel noise, we found it made no significant contribution to the error rates.
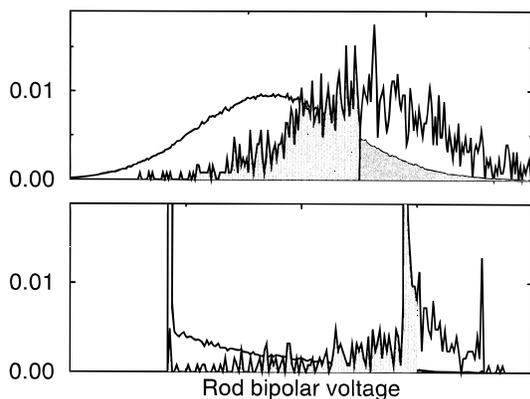
The threshold nonlinearity associated with the mGluR6 receptor and second-messenger cascade was found in the dogfish (Shiells & Falk, 1994). Since the mammalian rod bipolar cell is known to express the mGluR6 receptor and has a similar second-messenger cascade (de la Villa et al., 1995), it is plausible that the nonlinear threshold is present in mammals as well. Although the mGluR6 receptor has also been localized to membranes of the ON cone bipolar cells, it is likely that they do not contain such a threshold nonlinearity as they appear to collect and linearly sum graded signals from cones (e.g. Thibos & Werblin, 1978). According to the theory proposed by Shiells and Falk (1994), a small increase in the biochemical gain of the second-messenger cascade, c_{gain} in eqn. (5), can transform a gently saturating response to a sharply saturating one (see Fig. 5). Thus, with a small adjustment in biochemistry the same receptor and second-messenger cascade might operate in different modes in different cells. It is interesting to note that, whereas for the cone system there are both ON and OFF bipolars, there is no OFF rod bipolar cell. The OFF cone bipolar has an ionotropic glutamate receptor, which does not have a strong nonlinear character (Shiells & Falk, 1994).
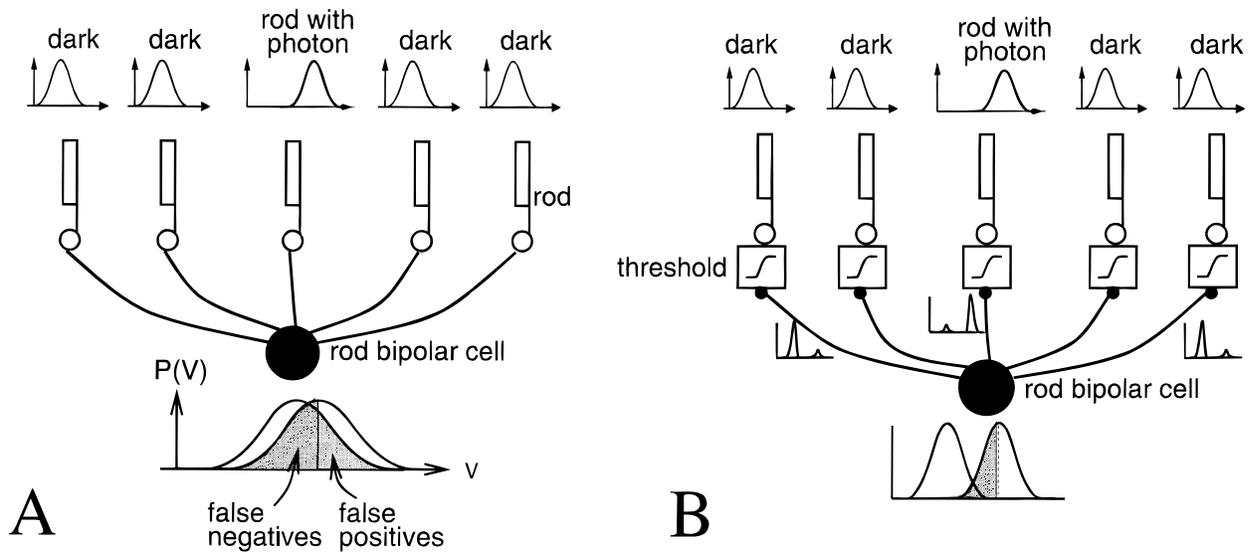
Fig. 9. How thresholding reduces errors. (A) The false positive rate increases due to convergence if the signals are linearly added. The rod voltage distribution is broadened by the continuous dark noise. The voltage distribution in the bipolar cell (lower curve) is shown for two cases: none of the rods absorbs a photon and one of the rods absorbs a photon. There is considerable overlap resulting in a high false positive rate (right shaded area). (B) If prior to summation the signal is thresholded, the distributions remain narrow and the summation does not strongly increase the false positive rate. The right shaded area (below the curve with maximum on the left, but right of the dashed line) is too small to be visible.

Setting the threshold

To obtain the low error rates reported for the model with a thresholding synapse, the threshold needed to be set accurately (±0.5 mV), and the same would be necessary in the retina. The type B horizontal cell axon terminal (HBAT) of cat is thought to provide GABAergic feedback to rods (Linberg & Fisher, 1988; Chun & Wässle, 1989; Vardi et al., 1994) and thus is a likely candidate to set the threshold. The HBAT receives input from

2000–3000 rods (Wässle et al., 1978), and thus even in the dark it receives a reasonably steady input from spontaneous isomerizations (0.01 Rh*/rod/s).

The precise mechanism of the feedback connection is unknown but there are two likely candidates: (1) feedback through GABA-A channels (Attwell et al., 1983), which would control depolarization of the rod terminal; and (2) modulation of the calcium-channel activation voltage of the rods by a GABA-B type mechanism (Gerschenfeld & Piccolino, 1980; Verweij et al., 1996), which would control calcium entry into the rod terminal. Both mechanisms would control transmitter release, and therefore would effectively set the threshold.

Evidence for thresholding operation

One might wonder if the nonlinear threshold mechanism implies a measurable nonlinearity in the scotopic light response of the rod bipolar or other postsynaptic neurons (AII amacrine, cone bipolar, ganglion cell). It does not because, although the nonlinearity reduces the single-photon response amplitude, this change precedes summation in the rod bipolar. After thresholding, photon events in the rod bipolar or downstream neurons can be summed linearly. At middle-to-high scotopic intensities, the photon events are numerous enough in these neurons to be temporally summed. Assuming that the thresholded photon events are of equal amplitude, the neuron's response can therefore be proportional to the photon flux.

At mesopic intensities, however, where two or more photon events pass simultaneously through a single rod synapse, a supralinearity might occur. This would happen shortly after the stimulus when the first photon response is above threshold, but before saturation sets in. The threshold would reduce the response to the first photon but not the response to a superimposed second photon. Hence, the two photon event would then have an amplitude greater than twice the single photon event (Fig. 12). Saturation of the peak

Fig. 10. Upper graph: Voltage distribution in the rod bipolar cell for the linear synapse. At left, distribution for the dark rods; at right, distribution for one rod capturing a photon and all others dark. The distributions are wide and have considerable overlap corresponding to the high false positive rate as indicated by the right shaded region. Left shaded region is false negative rate. Lower graph: Corresponding voltage distribution in the rod bipolar cell for the thresholding synapse. The distributions are sharply peaked, maximum is about 0.7 (not shown). Note that overlap is much less, so false positives are reduced.
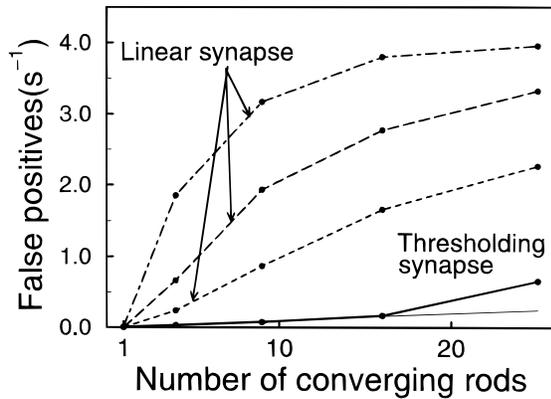
Fig. 11. False positive rate in the rod bipolar for multiple rods converging. The solid line: thresholding synapse, both noise sources present. Dotted-dashed: a linear synapse, both noise sources present. Dotted line: linear synapse, no vesicle release noise. Dashed line: linear synapse, no continuous dark noise. The dark light in the rod bipolar cell equals the single rod dark light times the number of rods converging (thin line). Vesicle release rate 100 vesicles/s; continuous dark noise 19%. The values for one rod are comparable to the dark light (0.01/s).

response would not much affect this mechanism because at early times the response is small. Evidence for just such a supralinearity in the rod bipolar response has recently been reported (Fig. 8A of Robson & Frishman, 1995), where the amplitude of the "derived PII" response at 40-ms latency was less than peak amplitude by one log unit but greater than expected on the basis of linearity by a factor of about 2. At later times, the bipolar cell shows a saturating response (Robson & Frishman, 1995) which might originate in saturation at the synapse or the soma.

Indirect evidence for the thresholding mechanism exists in ganglion cell physiology. In recordings of ganglion cells, the false positive rate was about equal to the dark event rate in single rods times the total number of rods converging onto the ganglion cell (Barlow et al., 1971; Mastronarde, 1983; Baylor et al., 1984; Ster-

ling et al., 1988). In our simulations with threshold, the false positive rate is proportional to the number of converging rods. These observations imply that at scotopic intensities the dark light is the major noise source at the ganglion cell and that the convergence introduced few extra errors, indicating that noise from other sources has been removed.

In addition, a ganglion cell receptive field surround can interact with the center in a nonlinear fashion (Wiesel & Hubel, 1966; Enroth-Cugell & Lennie, 1975; Barlow & Levick, 1976; Kaplan et al., 1979). At scotopic intensities, the ganglion cell's response to a light flashed in its surround is enhanced when the center is also stimulated with light. This type of interaction is consistent with a rod circuit that sums center and surround together before transmission through a nonlinear synapse. Such an interaction would occur if a rod surround signal generated by feedback from horizontal cells (e.g. the type B axon terminal in cat and rabbit) were passed through the rod synapse along with the single-photon signal.

Importance of nonlinear summation for the brain

The nonlinear summation described above is a general method to improve the performance of a neural circuit that sums spatially localized signals. For example, a complex cell in the primary visual cortex sums signals from its presynaptic neurons in a nonlinear fashion (Spitzer & Hochstein, 1985). The complex cell receives synaptic inputs from a large number of presynaptic neurons, and thus may encounter a noise problem similar to the one described here for the rod bipolar. The measured behavior can be described with a model with a threshold prior to the summation very similar to ours (Sakai & Tanaka, 1998). This suggests that a possible function of such nonlinear processing in the visual cortex could be noise removal.

Acknowledgments

References

Abramowitz, M. & Stegun, I.A. (1965). *Handbook of Mathematical Functions*. New York: Dover.

Ashmore, J.F. & Copenhagen, D.R. (1983). An analysis of transmission from cones to hyperpolarizing bipolar cells in the retina of the turtle. *Journal of Physiology* **340**, 569–597.

Ashmore, J.F. & Falk, G. (1982). An analysis of voltage noise in rod bipolar cells of the dogfish retina. *Journal of Physiology* **332**, 273–297.

Attwell, D., Wilson, F.S. & Wu, S.M. (1983). A sign-reversing pathway from rods to double and single cones in the retina of the tiger salamander. *Journal of Physiology* **336**, 313–333.

Barlow, H.B. & Levick, W.R. (1976). Threshold setting by the surround of cat retinal ganglion cells. *Journal of Physiology* **259**, 737–757.

Barlow, H.B., Levick, W.R. & Yoon, M. (1971). Responses to single quanta of light in retinal ganglion cells of the cat. *Vision Research* (Suppl.) **3**, 87–101.

Barrett, E.F. & Stevens, C.F. (1972a). The kinetics of transmitter release at the frog neuromuscular junction. *Journal of Physiology* **227**, 691–708.

Barrett, E.F. & Stevens, C.F. (1972b). Quantal independence and uniformity of presynaptic release kinetics at the frog neuromuscular junction. *Journal of Physiology* **227**, 665–689.

Baylor, D.A., Matthews, G. & Yau, K.W. (1980). Two components of electrical dark noise in toad retinal rod outer segments. *Journal of Physiology* **309**, 591–621.

Baylor, D.A., Nunn, B.J. & Schnapf, J.L. (1984). The photocurrent,

Fig. 12. At mesopic intensities the threshold can cause a supralinear response to a flash stimulus. Solid line: one-photon response, dashed line: two-photon response. At times shortly after photon absorption, the response of the bipolar cell to a two-photon signal at a single dendrite (upper arrow) is more than twice the single-photon response (lower arrow). At later times the effect is less strong and due to saturation effects (at the synapse or the soma) the response can become sublinear.

noise and spectral sensitivity of rods of the monkey *Macaca fascicularis*. *Journal of Physiology* **357**, 575–607.

BELGUM, J.H. & COPENHAGEN, D.R. (1988). Synaptic transfer of rod signals to horizontal and bipolar cells in the retina of the toad (*Bufo marinus*). *Journal of Physiology* **396**, 225–245.

CERVETTO, L. & PICCOLINO, M. (1974). Synaptic transmission between photoreceptors and horizontal cells in the turtle retina. *Science* **183**, 417–419.

CHUN, M.H. & WÄSSLE, H. (1989). Gaba-like immunoreactivity in cat retina: Electron microscopy. *Journal of Comparative Neurology* **279**, 55–67.

DACHEUX, R.F. & RAVIOLA, E. (1986). The rod pathway in the rabbit retina: A depolarizing bipolar and amacrine cell. *Journal of Neuroscience* **6**, 331–345.

DAVENPORT, W.B. & ROOT, W. L. (1958). *An Introduction to the Theory of Random Signals and Noise*. New York: McGraw-Hill.

DE LA VILLA, P., KURAHASHI, T. & KANEKO, A. (1995). L-glutamate-induced responses and cGMP-activated channels in three subtypes of retinal bipolar cells dissociated from the cat. *Journal of Neuroscience* **15**, 3571–3582.

DETWILER, P.B., HODGKIN, A.L. & LAMB, T.D. (1984). A note on the synaptic events in hyperpolarizing bipolar cells of the turtle's retina. In *Photoreceptors*, ed. BORSELLINO, A. & CERVETTO, L., pp. 285–293. New York: Plenum.

ENROTH-CUGELL, C. & LENNIE, P. (1975). The control of retinal ganglion cell discharge by receptive field surrounds. *Journal of Physiology* **247**, 551–578.

FAMIGLIETTI, E.V. & KOLB, H. (1975). A bistratified amacrine cell and synaptic circuitry in the inner plexiform layer of the retina. *Brain Research* **84**, 293–300.

FREED, M.A. (1998). Sustained synaptic release rate estimated from synaptic noise in a retinal ganglion cell (submitted).

FRISHMAN, L.J., REDDY, M.G. & ROBSON, J.G. (1996). Effects of background light on the human dark-adapted electroretinogram and psychophysical threshold. *Journal of the Optical Society of America A* **13**, 601–612.

GERSCHENFELD, H.M. & PICCOLINO, M. (1980). Sustained feedback effects of l-horizontal cells on turtle cones. *Proceedings of the Royal Society B* (London) **206**, 465–480.

GRÜNERT, U., MARTIN, P.R. & WÄSSLE, H. (1994). Immunocytochemical analysis of bipolar cells in the macaque monkey retina. *Journal of Comparative Neurology* **348**, 607–627.

KANEKO, A. (1979). Physiology of the retina. *Annual Review of Neuroscience* **2**, 169–191.

KAPLAN, E., MARCUS, S. & SO, Y.T. (1979). Effects of dark adaptation on spatial and temporal properties of receptive fields in cat lateral geniculate nucleus. *Journal of Physiology* **294**, 561–580.

KATZ, B. & MILEDI, R. (1965). The measurements of synaptic delay, and the time course of acetylcholine release at the neuromuscular junction. *Proceedings of the Royal Society B* (London) **161**, 483–495.

LAMB, T.D. (1990). Dark adaptation: A re-examination. In *Night Vision: Basic, Clinical, and Applied Aspects*, ed. HESS, R.F., SHARPE, L.T. & NORDBY, K., pp. 177–222. New York: Cambridge.

LANKHEET, M.J.M., ROWE, M.H., VAN WEZEL, R.J.A. & VAN DE GRIND, W.A. (1996). Spatial and temporal properties of cat horizontal cells after prolonged dark adaptation. *Vision Research* **36**, 3955–3967.

LAUGHLIN, S.B. & DE RUYTER VAN STEVENINCK, R.R. (1996). Measurements of signal transfer and noise suggest a new model for graded transmission at an adapting retinal synapse. *Journal of Physiology* **494**, 19 (Abstract).

LEVICK, W.R., THIBOS, L.N., COHN, T.E., CATANZARO, D. & BARLOW, H.B. (1983). Performance of cat retinal ganglion cells at low light level. *Journal of General Physiology* **82**, 405–426.

LINBERG, K.A. & FISHER, S.K. (1988). Ultrastructural evidence that horizontal cell axon terminals are presynaptic in human retina. *Journal of Comparative Neurology* **268**, 281–287.

MAKOUS, W. (1990). Absolute sensitivity. In *Night Vision: Basic, Clinical, and Applied Aspects*, ed. HESS, R.F., SHARPE, L.T. & NORDBY, K., pp. 146–176. New York: Cambridge.

MAPLE, B.R., WERBLIN, F.S. & WU, S.M. (1994). Miniature excitatory postsynaptic currents in bipolar cells of the tiger salamander retina. *Vision Research* **34**, 2357–2362.

MASTRONARDE, D.N. (1983). Correlated firing of cat retinal ganglions cells: II. responses of X- and Y-cell to single quantal events. *Journal of Neurophysiology* **49**, 325–349.

NAWY, S. & JAHR, C.E. (1990). Suppression by glutamate of cGMP-activated conductance in retinal bipolar cells. *Nature* **346**, 269–271.

NAWY, S. & JAHR, C.E. (1991). cGMP-gated conductance in retinal bipolar cells is suppressed by the photoreceptor transmitter. *Neuron* **7**, 677–683.

NELSON, R. (1982). AII amacrine cells quicken time course of rod signals in the cat retina. *Journal of Neurophysiology* **47**, 928–947.

PUGH, E.N. & ALTMAN, J. (1988). A role for calcium in adaptation. *Nature* **334**, 16–17.

RAO-MIROTZNIK, R. & STERLING, P. (1998). *Transmitter concentration at a three dimensional synapse* (submitted).

RAO, R., BUCHSBAUM, G. & STERLING, P. (1994). Rate of quantal transmitter release at the mammalian rod synapse. *Biophysical Journal* **67**, 57–64.

RAVIOLA, E. & GILULA, N.B. (1973). Gap junctions between photoreceptor cells in the vertebrate retina. *Proceedings of the National Academy of Sciences of the U.S.A.* **70**, 1677–1681.

ROBSON, J.G. & FRISHMAN, L.J. (1995). Response linearity and kinetics of the cat retina: The bipolar component of the dark-adapted electroretinogram. *Visual Neuroscience* **12**, 837–850.

SAKAI, K. & TANAKA, S. (1998). Computational mechanisms underlying the second-order structure of cortical complex cells. In *Computational Neuroscience: Trends in Research, 1998*, ed. BOWER, J.M. New York: Plenum (in press).

SAKITT, B. (1972). Counting every quantum. *Journal of Physiology* **223**, 131–150.

SCHNEEWEIS, D.M. & SCHNAPF, J.L. (1995). Photovoltage in rods and cones in the macaque retina. *Science* **268**, 1053–1056.

SHIELLS, R.A. & FALK, G. (1990). Glutamate receptors of rod bipolar cells are linked to a cyclic GMP cascade via a G-protein. *Proceedings of the Royal Society B* (London) **242**, 91–94.

SHIELLS, R.A. & FALK, G. (1994). Responses of rod bipolar cells isolated from dogfish retinal slices to concentration jumps of glutamate. *Visual Neuroscience* **11**, 1175–1183.

SIEVING, P.A., FRISHMAN, L.J. & STEINBERG, R.H. (1986). Scotopic threshold response of proximal retina in cat. *Journal of Neurophysiology* **56**, 1049–1061.

SMITH, R.G. (1992). NeuronC: A computational language for investigating functional architecture of neural circuits. *Journal of Neuroscience Methods* **43**, 83–108.

SMITH, R.G. & VARDI, N. (1995). Simulation of the AII amacrine cell of mammalian retina: Functional consequences of electrical coupling and regenerative membrane properties. *Visual Neuroscience* **12**, 851–860.

SMITH, R.G., FREED, M.A. & STERLING, P. (1986). Microcircuitry of the dark-adapted cat retina: Functional architecture of the rod–cone network. *Journal of Neuroscience* **6**, 3505–3517.

SPITZER, H. & HOCHSTEIN, S. (1985). A complex-cell receptive-field model. *Journal of Neurophysiology* **53**, 1266–1286.

STERLING, P., FREED, M. & SMITH, R.G. (1988). Architecture of rod and cone circuits to the on-beta ganglion cell. *Journal of Neuroscience* **8**, 623–642.

STEVENS, C.F. (1993). Quantal release of neurotransmitter and long-term potentiation. *Cell* (Suppl.) **72**, 55–63.

TAMURA, T., NAKATANI, K. & YAU, K.-W. (1989). Light adaptation in cat retinal rods. *Science* **245**, 755–758.

TESSIER-LAVIGNE, M. & ATTWELL, D. (1988). The effect of photoreceptor coupling and synapse nonlinearity on signal:noise ratio in early visual processing. *Proceedings of the Royal Society B* (London) **234**, 171–197.

THIBOS, L.N. & WERBLIN, F.A. (1978). The response properties of the steady antagonistic surround in the mudpuppy retina. *Journal of Physiology* **278**, 79–99.

TRIFONOV, Y.A. (1968). Study of synaptic transmission between the photoreceptor and the horizontal cell using electrical stimulation of the retina. *Biofizika* **13**, 809–817.

VAN TREES, H.L. (1968). *Detection, Estimation, and Modulation Theory I.* New York: Wiley.

VARDI, N., KAUFMAN, D.L. & STERLING, P. (1994). Horizontal cells in cat and monkey retina express different isoforms of glutamic acid decarboxylase. *Visual Neuroscience* **11**, 135–142.

VARDI, N., MATESIC, D.F., MANNING, D.R., LIEBMAN, P.A. & STERLING, P. (1993). Identification of a G-protein in depolarizing rod bipolar cells. *Visual Neuroscience* **10**, 473–478.

VERWEIJ, J., KAMERMANS, M. & SPEKREISE, H. (1996). Horizontal cells feed back to cones by shifting the cone calcium-current activation range. *Vision Research* **36**, 3943–3953.

von Gersdorff, H., Vardi, E., Matthews, G. & Sterling, P. (1996). Evidence that vesicles on the synaptic ribbon can be rapidly released. *Neuron* **16**, 1–20.

Wässle, H., Boycot, B.B. & Peichl, L. (1978). Receptor contacts of horizontal cells in the retina of the domestic cat. *Proceedings of the Royal Society B* (London) **203**, 247–267.

Wässle, H., Yamashita, M., Greferath, U., Grünert, U. & Müller, F. (1991). The rod bipolar cell of the mammalian retina. *Visual Neuroscience* **7**, 99–112.

Wiesel, T.N. & Hubel, D.N. (1966). Spatial and chromatic interactions in the lateral geniculate body of the rhesus monkey. *Journal of Neuroscience* **29**, 1115–1156.

Yamashita, M. & Wässle, H. (1991). Responses of rod bipolar cells isolated from the rat retina to the glutamate agonist 2-amino-4-phosphono-buteric acid (apb). *Journal of Neuroscience* **11**, 2372–2382.

Young, H.M. & Vaney, D.I. (1991). Rod-signal interneurons in the rabbit retina: 1. Rod bipolar cells. *Journal of Comparative Neurology* **310**, 139–153.

Appendix: Ideal discriminator analysis

Single rod

In this section, we develop a theoretical model which shows the advantage of a nonlinearity above a linear synapse for the performance of the system. First, consider a single rod connected to the rod bipolar. The noise in the rod bipolar cell has two major components: the vesicle noise and the rod continuous dark noise. We assume here that the sum of the noises has a Gaussian distribution and that its variance in the absence of a signal is the same as in the presence of a signal. The probability distribution of the voltage in the rod bipolar after averaging over the integration time is

$$p_0(V) = \frac{1}{\sigma\sqrt{2\pi}} \, e^{-V^2/2\sigma^2}, \qquad (A1)$$

when there is no signal present (the average was set to zero for convenience). If a photon is captured, the distribution is

$$p_1(V) = \frac{1}{\sigma\sqrt{2\pi}} \, e^{-(V-\bar{V})^2/2\sigma^2}. \qquad (A2)$$

Here $\bar{V}$ stands for the average response to a detected photon; σ is the standard deviation in the time-integrated signal. Next, we introduce a discrimination voltage V_{disc} in order to discriminate between the absence and presence of a signal. If the averaged voltage is higher than this voltage, we decide that a signal was present, if the voltage is lower no signal was present. Due to the noise, the two distributions overlap which introduces the possibility that the signal might be detected incorrectly (Fig. 9). The probability of a false positive (FP) and false negative (FN) is, respectively,

$$FP(V_{\text{disc}}) = \frac{1}{\sigma\sqrt{2\pi}} \int_{V_{\text{disc}}}^{\infty} e^{-V^2/2\sigma^2} = \frac{1}{2}\,\text{erfc}\!\left(\frac{V_{\text{disc}}}{\sqrt{2}\sigma}\right), \quad (A3)$$

$$FN(V_{\text{disc}}) = \frac{1}{\sigma\sqrt{2\pi}} \int_{-\infty}^{V_{\text{disc}}} e^{-(V-\bar{V})^2/2\sigma^2}$$

$$= \frac{1}{2} + \frac{1}{2}\,\text{erf}\!\left(\frac{V_{\text{disc}} - \bar{V}}{\sqrt{2}\sigma}\right). \qquad (A4)$$

There are various possibilities for setting the discrimination voltage. Because at low scotopic light levels photons are rare, it is

advantageous to set the discrimination voltage such that it gives a low false positive rate. This leads to a high *FN*-rate or, equivalently, a low quantum efficiency. Note that this is somewhat counterintuitive as one might expect that at low light levels the retina would try to catch every signal; however, in that case the signal would drown between false positive signals and would be useless.

We fix the discrimination voltage such that the false negative rate equals 50%, or, equivalently, the quantum efficiency of the circuit is 50%. This implies that the discrimination voltage is fixed at $V_{\text{disc}} = \bar{V}$. The false positive rate is the performance measure for the system.

A more elaborate analysis would be, for example, to minimize the total number of errors, which equals the false positive rate times the number of dark events plus false negative rate times the number of photon events (van Trees, 1968). The optimal threshold would then vary with the mean intensity level and the number of converging rods.

We note that the false positive and negative rates can also be analyzed with Receiver Operating Characteristics (ROC). The ROC curves are found by parametrically plotting of *FP versus* $1 - FN$ with the threshold voltage as the varying parameter. This method was applied to ganglion cells by Levick et al. (1983).

The convergence of many rods

Consider the convergence of N rods at a single rod bipolar. Because the signal is rare only two cases occur: (1) none of the rods carries signal, or (2) one rod carries signal while the others do not. Suppose first that at the rod bipolar the signals are linearly summed (with equal weights). Summing Gaussian distributions yields a new Gaussian distribution with a mean equal to the sum of the means and a variance equal to the sum of the variances; thus the standard deviation increases by a factor $\sqrt{N}$. If none of the rods carries a signal, this distribution will be

$$p_0(V) = \frac{1}{\sigma\sqrt{2\pi N}} \, e^{-V^2/2N\sigma^2}. \qquad (A5)$$
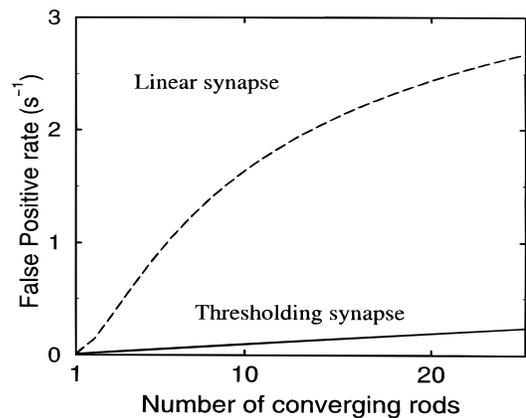
Fig. 13. The false positive rate as a function of number of converging rods according to the theoretical model. For a linear synapse, the false positive rate grows initially exponentially with the number of rods (dashed curve). With an ideal thresholding synapse, the false positive rate is linear in the number of rods (solid line). The noise was set such that the false positive rate for $N = 1$ was 0.01 event/rod/s for both curves; the false negative rate was fixed at 50%, 100-ms integration time.

If one rod receives a signal, the distribution is

$$p_1(V) = \frac{1}{\sigma\sqrt{2\pi N}} e^{-(V-\bar{V})^2/2N\sigma^2},$$ (A6)

see Fig. 10. The chances for a false positives and negatives becomes now, respectively,

$$FP_N = \frac{1}{2}\,\mathrm{erfc}\left(\frac{V_{\mathrm{disc}}}{\sqrt{2N}\sigma}\right),$$ (A7)

$$FN_N = \frac{1}{2} + \frac{1}{2}\,\mathrm{erf}\left(\frac{V_{\mathrm{disc}} - \bar{V}}{\sqrt{2N}\sigma}\right).$$ (A8)

Due to the convergence, the voltage distributions, eqns. (A5–A6), are somewhat wider, yet the false positive rate, eqn. (A7), increases drastically (Fig. 9). For small rates FP_N, the error function can be approximated as $\mathrm{erfc}(V_{\mathrm{disc}}/\sqrt{N}) \sim \sqrt{N}e^N$. The false positive rate in the bipolar cell thus initially rises exponentially with the number of converging rods.

Threshold nonlinearity

Now suppose that there is a threshold nonlinearity present. The best location for the nonlinearity is before the signal summation. The continuous distribution is transformed into two narrow probability distributions (Fig. 9).

In the limit of very narrow peaks, the chance for a false positive is given by one minus the chance that all rod signals are transmitted correctly:

$$FP_N = 1 - (1 - FP)^N,$$ (A9)

$$= 1 - \left[\frac{1}{2} + \frac{1}{2}\,\mathrm{erf}\left(\frac{V_{disc}}{\sqrt{2}\sigma}\right)\right]^N,$$ (A10)

$$\approx N.FP \qquad (FP \ll 1).$$ (A11)

The false negative rate is obtained by considering the case where one input signal is missed, and the other rods cause no FP signal.

$$FN_N = FN(1 - FP)^{N-1},$$ (A12)

$$= \left[\frac{1}{2} + \frac{1}{2}\,\mathrm{erf}\left(\frac{V_{disc} - \bar{V}}{\sqrt{2}\sigma}\right)\right]\left[\frac{1}{2} + \frac{1}{2}\,\mathrm{erf}\left(\frac{V_{disc}}{\sqrt{2}\sigma}\right)\right]^{N-1},$$ (A13)

$$\approx FN \qquad (FP \ll 1).$$ (A14)

At low false positive rates, the false positive rate in the rod bipolar is proportional to the number of rods [eqn. (A11)]. The false negative rate is in first approximation unchanged; eqn. (A14). The nonlinearity does not remove the errors already present, but it reduces the increase in errors due to the convergence. Also note that for a single rod ($N = 1$), the error rate of the linear and the thresholding synapse are the same.

With one rod, the false positive rate of both types of synapses is the same, but with more rods converging the increase in the false positive rate is much greater for the linear synapse (Fig. 13).